Transition of Boundary Layer on a Circular Cylinder in Uniform Flow

Suresh Behara, Sanjay Mittal*

Department of Aerospace Engineering
Indian Institute of Technology Kanpur, 208016, India
sureshb@iitk.ac.in, smittal@iitk.ac.in*

Abstract. The boundary layer on a circular cylinder in a uniform flow undergoes a transition from a laminar to turbulent state at $Re \sim 1 \times 10^5$. The effect of placing a roughness element on one side of the cylinder to hasten the transition is investigated via two-dimensional numerical simulations. Results are presented for the effect of roughness on the aerodynamic forces for a variety of Reynolds numbers. A substantial decrease in the drag coefficient is observed as the Reynolds number is increased beyond the critical value. In the case of cylinder with roughness the decrease is achieved in two steps due to the staggered transition of the boundary layer on the upper and lower sides. Reversal of lift is also observed during the transition.

Key words: Boundary layer, transition to turbulence, pressure distribution, drag, lift.

1. Introduction

The flow past a circular cylinder has been a focus of research for long time. However, there are a few questions that are still not completely answered. One of them is regarding the transition of the boundary layer. The flow in the far and near wake undergoes a transition process at Re as low as 200. However, for a cylinder with smooth surface, the boundary layer stays laminar upto $Re \sim 10^5$. Achenbach *et al.* [1981], Guven *et al.* [1980] carried out experimental studies on cylinder with distributed roughness at a variety of Reynolds numbers. The roughness significantly influences the transition process of the boundary layer. Their studies focused on the influence of the surface roughness on certain characteristics of the flow such as Strouhal number, pressure distribution on the cylinder surface etc. It is well known that the surface roughness hastens the transition of the boundary layer. Also, compared to a laminar state, a turbulent boundary layer delays the separation of the flow on the cylinder surface. In order to simulate the flow characteristics at high Reynolds numbers, Nakamura *et al.* [1982] carried out experimental investigations by placing roughness strips on the surface of a cylinder. Later, Nebres and Batill [1992] studied the effect of the angular position and height of the roughness element. Kareem and Cheng [1999], in their experiments, placed discrete roughness elements at four different locations on the cylinder surface. With this arrangement they simulated the pressure field, obtained at trans-critical Reynolds numbers, performing experiments at Re as low as 2.5×10^4. More recently, Alam *et al.* [2003] obtained reduction in fluid forces acting on a circular cylinder by placing tripping rods on the surface of the cylinder. They investigated the effect of tripping rods of

three different diameters placed at various angular positions. They observed that the optimum angular position to reduce the fluid forces on the cylinder is 30^0 from the front stagnation point.
The present numerical study is intended to investigate the effect of adding a surface roughness element on only one side of the cylinder on the aerodynamic force coefficients. 2D numerical simulations have been carried out for, both, the smooth cylinder and the one with a roughness element. The roughness element, a protrusion of height 0.5% of the cylinder diameter is placed on the upper side at an angle 55^0 from the front stagnation point. The incompressible flow equations are solved by a stabilized finite element formulation in two dimensions. A hybrid mesh with a structured band of elements close to the cylinder and an unstructured mesh in the remaining domain, generated via Delaunay's triangulation, is utilized. This way adequate resolution to capture the dynamics of the boundary layer upto $Re \sim 10^6$ is provided while still keeping the computational costs to a reasonable level. For the cylinder with a roughness element the mesh consists of 118, 609 nodes and 236, 364 triangular elements.

2. Governing equations and fem formulation

2.1. The Navier-Stokes equations

The Navier-Stokes equations governing incompressible fluid flow are

$$\rho(\frac{\partial \mathbf{u}}{\partial t} + \mathbf{u} \cdot \boldsymbol{\nabla}\mathbf{u} - \mathbf{f}) - \boldsymbol{\nabla} \cdot \boldsymbol{\sigma} = 0 \qquad \text{on } \Omega_t \times \ (0,T), \tag{1}$$

$$\boldsymbol{\nabla} \cdot \mathbf{u} = 0 \qquad \text{on } \Omega_t \times \ (0,T). \tag{2}$$

Here ρ, $\mathbf{u}$, $\mathbf{f}$ and $\boldsymbol{\sigma}$ are the density, velocity, body force and the stress tensor, respectively. The stress tensor comprises the sum of its isotropic and deviatoric parts as shown below:

$$\boldsymbol{\sigma} = -p\mathbf{I} + \mathbf{T}, \quad \mathbf{T} = 2\mu\boldsymbol{\varepsilon}(\mathbf{u}), \quad \boldsymbol{\varepsilon}(\mathbf{u}) = \tfrac{1}{2}((\boldsymbol{\nabla}\mathbf{u}) + (\boldsymbol{\nabla}\mathbf{u})^T), \tag{3}$$

where p, $\mathbf{I}$ and μ are the pressure, identity tensor and dynamic viscosity, respectively. Dirichlet and Neumann-type boundary conditions are represented as

$$\mathbf{u} = \mathbf{g} \ on \ (\Gamma)_g, \quad \mathsf{n} \cdot \boldsymbol{\sigma} = \mathbf{h} \ on \ (\Gamma)_h, \tag{4}$$

where $(\Gamma)_g$ and $(\Gamma)_h$ are the subsets of the boundary Γ and n is its unit normal vector. The initial condition on the velocity is specified on Ω at $t = 0$:

$$\mathbf{u}(\mathbf{x}, 0) = \mathbf{u}_0 \quad on \ \Omega_0, \tag{5}$$

where $\mathbf{u}_0$ is divergence free.

2.2. Semi-discrete finite element formulation

The Navier-Stokes equations are solved for the flow in a 2D domain Ω, and this domain is discretized into sub domains Ω^e, where, $e = 1, 2, ..., n_{el}$ and n_{el} is the number of elements. On the boundary, Γ, of the domain Dirichlet and Neumann boundary conditions have been applied. For velocity and pressure, trial functions

are taken from finite element spaces $\mathcal{S}_{\mathbf{u}}^h$ and $\mathcal{S}_{\mathbf{p}}^h$, and weighting functions are from $\mathcal{V}_{\mathbf{u}}^h$ and $\mathcal{V}_{\mathbf{p}}^h$. These function spaces are defined as follows:

$$\mathcal{S}_{\mathbf{u}}^h = \{\mathbf{u}^h | \mathbf{u}^h \in H^{1h}(\Omega), \mathbf{u}^h \doteq \mathbf{g}^h \quad \text{on} \quad \Gamma_g\}, \tag{6}$$

$$\mathcal{V}_{\mathbf{u}}^h = \{\mathbf{w}^h | \mathbf{w}^h \in H^{1h}(\Omega), \mathbf{w}^h \doteq 0 \quad \text{on} \quad \Gamma_g\}, \tag{7}$$

$$\mathcal{S}_{\mathbf{p}}^h = \mathcal{V}_{\mathbf{p}}^h = \{q^h | q^h \in H^{1h}(\Omega)\}. \tag{8}$$

$H^{1h}(\Omega)$ represents the finite-dimensional function space. The semi-discrete finite element formulation is given as follows: find $\mathbf{u}^h \in \mathcal{S}_{\mathbf{u}}^h$ and $p^h \in \mathcal{S}_{\mathbf{p}}^h$ such that $\forall \mathbf{w}^h \in \mathcal{V}_{\mathbf{u}}^h$, $q^h \in \mathcal{V}_p^h$,

$$\begin{aligned}\int_\Omega \mathbf{w}^h \cdot \rho \left(\frac{\partial \mathbf{u}^h}{\partial t} + \mathbf{u}^h \cdot \boldsymbol{\nabla} \mathbf{u}^h - \mathbf{f} \right) d\Omega + \int_\Omega \boldsymbol{\varepsilon}(\mathbf{w}^h) : \boldsymbol{\sigma}(p^h, \mathbf{u}^h) d\Omega + \int_\Omega \mathbf{q}^h \boldsymbol{\nabla} \cdot \mathbf{u}^h d\Omega \\ + \sum_{e=1}^{n_{el}} \int_{\Omega^e} \frac{1}{\rho} (\boldsymbol{\tau}_{SUPG} \rho \mathbf{u}^h \cdot \boldsymbol{\nabla} \mathbf{w}^h + \boldsymbol{\tau}_{PSPG} \boldsymbol{\nabla} \mathbf{q}^h) \cdot \\ \left[\rho \left(\frac{\partial \mathbf{u}^h}{\partial t} + \mathbf{u}^h \cdot \boldsymbol{\nabla} \mathbf{u}^h - \mathbf{f} \right) - \boldsymbol{\nabla} \cdot \boldsymbol{\sigma}(p^h, \mathbf{u}^h) \right] d\Omega^e \\ + \sum_{e=1}^{n_{el}} \int_{\Omega^e} \delta \boldsymbol{\nabla} \cdot \mathbf{w}^h \rho \boldsymbol{\nabla} \cdot \mathbf{u}^h d\Omega^e = \int_{\Gamma_h} \mathbf{w}^h \cdot \mathbf{h}^h d\Gamma \end{aligned} \tag{9}$$

For enhancing numerical stability SUPG (Streamline-Upwind/Petrov-Galerkin) and PSPG (Pressure-Stabilizing/Petrov-Galerkin) terms (Tezduyar *et al.* [1992]) are added in the form of first series of elemental level integrals to the variational formulation, shown above. Time integration of the above equations is done via the, second order in time accurate, generalized trapezoidal rule.
Aerodynamic forces are obtained, integrating the pressure and viscous stresses around the circumference of the cylinder, as given below:

$$C_D = \frac{1}{\frac{1}{2}\rho U_\infty^2 D} \int_{\Gamma_{cyl}} (\boldsymbol{\sigma} \mathsf{n}) \cdot \mathsf{n}_\mathsf{x} d\Gamma \tag{10}$$

$$C_L = \frac{1}{\frac{1}{2}\rho U_\infty^2 D} \int_{\Gamma_{cyl}} (\boldsymbol{\sigma} \mathsf{n}) \cdot \mathsf{n}_\mathsf{y} d\Gamma. \tag{11}$$

Here n_x and n_y are the cartesian components of the unit vector$\mathsf{n}$ that is normal to the cylinder boundary Γ_{cyl}.

2.3. Results and discussion

Computations have been carried out at Reynolds numbers ranging from 1×10^4 to 1×10^6. Figure 1 shows the variation of the drag and lift coefficients with Re for the smooth cylinder and the one with roughness element. From this figure it can be observed that the phenomenon of "drag-crisis" has been captured quite well with the present computations. Overall, the presence of roughness element leads to lowering of the critical Re for the onset of transition. Unlike the smooth cylinder, the one with roughness element shows the drop in C_D in two stages. In the first stage, which is rather rapid, the flow on the upper side goes through a transition beyond $Re \sim 2 \times 10^4$ while the flow on the lower side still remains laminar. With the increase

in Re beyond $Re \sim 2 \times 10^4$ on the upper side the boundary layer undergoes critical state. In this state, laminar separation and further turbulent reattachment takes place. This phenomenon delays the separation of the boundary layer on the upper side reducing the size of the near wake. Hence with the separation point moving downstream, drag decreases rapidly. In the first stage of the drag crisis pressure on the upper side decreases due to the transition of the boundary layer to a turbulent state via shear layer instabilities (Singh & Mittal [2005]). Figure 2 shows the C_P distribution for, both, the smooth cylinder and the one with roughness element.

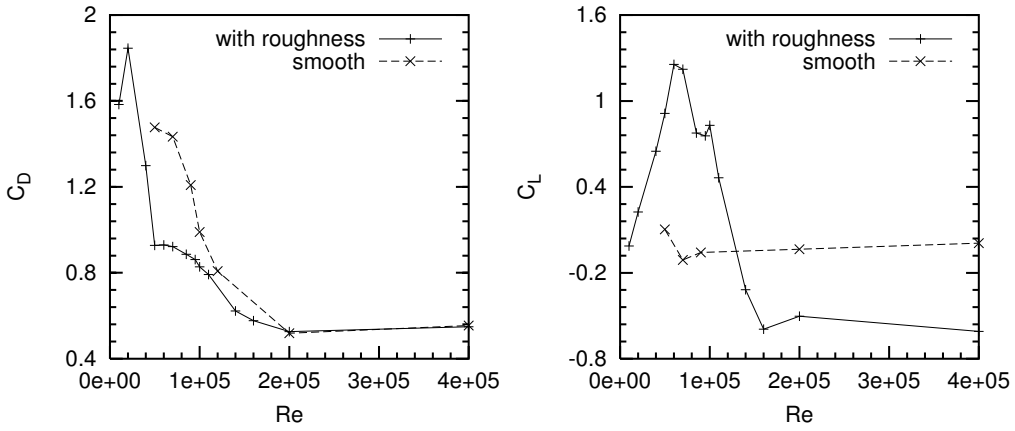

Figure 1. Variation of C_D and C_L with Re on the smooth cylinder and the one with roughness element on the upper side.

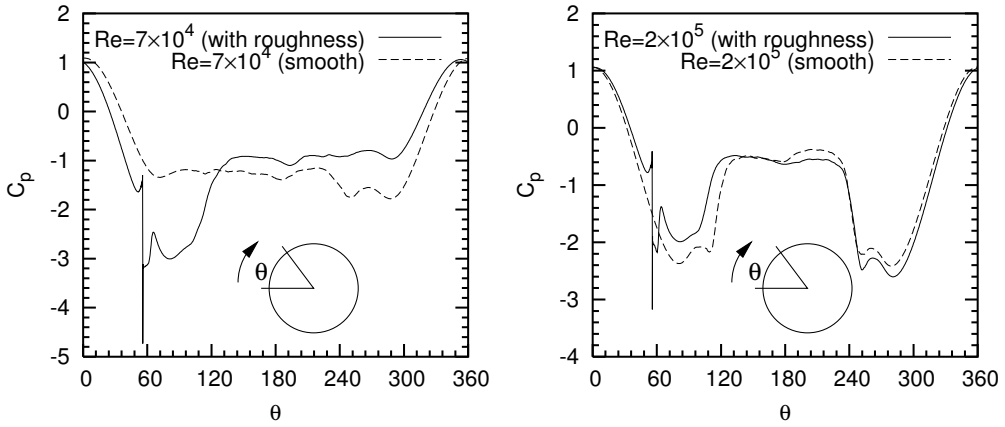

Figure 2. C_P distribution on the surfaces of the smooth cylinder and the one with roughness element at $Re = 7 \times 10^4$ and 2×10^5.

From this figure it can be noticed that the difference in C_P on the upper and lower sides of the smooth cylinder is negligible since the flow is symmetric. However, for the case with roughness element at $Re = 7 \times 10^4$, C_P on the upper side becomes as low as -4.9 due to the presence of a recirculation bubble just downstream of the roughness element. Shortly downstream, it recovers because of the reattachment of the flow and rises to nearly -3.0. On the lower side of the cylinder, higher value of C_P is observed since the flow is laminar. This difference in pressure leads to net positive lift as seen in the C_L vs Re plot in Figure 1. As the Reynolds number is increased beyond $Re \sim 8 \times 10^4$ the boundary layer on the lower side also undergoes transition process and the separation point moves toward downstream. This phenomenon further reduces the size of the near wake. Consequently, drag

decreases further. In this phase, with the boundary layer on both the sides in critical state, the flow becomes symmetric and the lift approaches a zero value. When Re is increased further, the flow on the upper side achieves a super-critical state, while, on the lower side it still remains in the critical state. In the super-critical state the separation point again moves a bit upstream toward the shoulder of the cylinder. In this state the pressure on the upper side is slightly higher than the pressure on the lower side. This can be observed from the C_P distribution at $Re = 2 \times 10^5$ in the figure 2. This now results in reversal of the lift and can be observed in Figure 1. At the same time, in the case of smooth cylinder boundary layer on both the sides is in the critical state leading to symmetric pressure distribution. Consequently, lift is zero on the smooth cylinder. The lift coefficient on the cylinder with roughness element is expected to go back to near zero once the flow becomes super-critical on both the sides.

3. Conclusions

The effect of a roughness element on the surface of the cylinder on the flow has been investigated. It lowers the critical Re for the transition and leads to asymmetry in the flow. The drop in C_D with Re occurs in two stages. In the first stage the flow becomes turbulent on the upper side and stays laminar on the lower side giving rise to positive lift. In the second stage the boundary layer on the lower side also undergoes transition. Lift reversal is observed when the flow on the upper side achieves a super- critical state.

References

[1] Achenbach, E. and Heinecke, E., On vortex shedding from smooth and rough cylinders in the range of Reynolds number 6×10^3 and 5×10^6. *J. Fluid Mech.,***109** (1981) 239–252.

[2] Guven, O., Farell, C. and Patel, V.C., Surface-roughness effects on the mean flow past circular cylinders. *J. Fluid Mech.,***98** (1980) 673–701.

[3] Nakamura, Y., Tomonari, Y., The effects of surface roughness on the flow past circular cylinders at high Reynolds numbers. *J. Fluid Mech.,***123** (1982) 363–378.

[4] Nebres, J., Batill, S., Flow about a circular cylinder with a single large-scale surface perturbation. *Exp. Fluid.,***15** (1993) 369–379.

[5] Kareem, A. and Cheng, C.M., Pressure and force fluctuations on isolated roughened circular cylinders of finite height in boundary layer flows. *J. Fluids Structs.,* **13** (1999) 907–933.

[6] Mahbub Alam, Md., Sakamoto, H. and Moriya, M., Reduction of fluid forces acting on a single circular cylinder and two circular cylinders by using tripping rods. *J. Fluids Structs.,***18** (2003) 347–366.

[7] Singh, S.P. and Mittal, S., Flow past a cylinder: shear layer instability and drag crisis. *Int. J. Num. Meth. Fluids.,* **47** (2005) 75–98.

[8] Tezduyar, T.E., Mittal, S., Ray, S.E., and Shih, R., Incompressible flow computations with stabilized bilinear and linear equal order interpolation velocity pressure elements. *Comp. Meth. Appl. Mech.,* **95** (1992) 221–242.